Dynamical tropopause based on isentropic potential vorticity gradients

A. Kunz,[1,2] P. Konopka,[1] R. Müller,[1] and L. L. Pan[3]

Received 9 April 2010; revised 14 September 2010; accepted 21 September 2010; published 14 January 2011.

[1] Since its inception, the dynamical tropopause based on potential vorticity (PV) is identified by the PV gradient on isentropes. Conceptually, significant isentropic gradients shown on the middle world PV maps reflect the underlying transport barrier associated with the tropopause, formed by jet streams that separate tropospheric air masses at low latitudes and stratospheric air masses at high latitudes. Largely owing to the lack of a general method, the dynamical tropopause has often been represented by a PV value chosen ad hoc without any temporal or spatial differentiation. In this work, we present a method for determining the PV isoline of the dynamical tropopause based on the isentropic PV gradients. Using 1 year of data from the European Centre for Medium–Range Weather Forecasts, the spatial and temporal variability of this PV gradient-based dynamical tropopause is examined. The results show that in general there is a broad distribution of PV values at the dynamical tropopause, ranging from 1.5 to 5 potential vorticity units. Therefore, a fixed PV surface for all isentropes and seasons does not accurately represent the location of the "tropopause barrier." The PV at the dynamical tropopause increases with increasing potential temperature. This increase is more pronounced in the Southern Hemisphere than in the Northern Hemisphere. The seasonal cycle shows higher PV values at the dynamical tropopause during summer than during winter. This seasonal cycle is larger on higher isentropes. The dispersion of the PV at the dynamical tropopause about its mean is twofold larger during summer and autumn than during winter and spring in both hemispheres.

Citation: Kunz, A., P. Konopka, R. Müller, and L. L. Pan (2011), Dynamical tropopause based on isentropic potential vorticity gradients, *J. Geophys. Res.*, *116*, D01110, doi:10.1029/2010JD014343.

1. Introduction

[2] The tropopause separates the well-mixed troposphere from the stratified stratosphere. The increase of static stability across the tropopause demonstrates that the troposphere and the stratosphere are air volumes with different thermal stratification [*Holton et al.*, 1995]. Different definitions for the tropopause exist which are based on different concepts [*Hoinka*, 1997]. The conventional definition is the thermal tropopause, which is based on the vertical temperature lapse rate [*World Meteorological Organization* (*WMO*), 1957]. The original concept of the dynamical tropopause was based on the isentropic gradient of potential vorticity (PV) [*Reed*, 1955], but it has been most often represented by a particular PV surface to simplify matters [e.g., *Hoskins et al.*, 1985; *WMO*, 1986; *Holton et al.*, 1995].

[3] PV contains both dynamic (absolute vorticity) and thermodynamic (potential temperature) properties and is a conserved quantity in the absence of diabatic heating or cooling and frictional forces [*Ertel*, 1942]. The PV threshold between the troposphere and the stratosphere, which defines the dynamical tropopause, is positive in the Northern Hemisphere and negative in the Southern Hemisphere. PV does not provide a well-defined dynamical tropopause for the tropics and is only used in the extratropics [see, e.g., *Holton et al.*, 1995].

[4] There is no universally used PV threshold for the dynamical tropopause, but the most common choice is the 2 PVU surface (1 PVU = 10^{-6} K m^2 kg^{-1} s^{-1}, standard potential vorticity unit) [e.g., *Holton et al.*, 1995]. *Hoerling et al.* [1991] found that the 3.5 PVU isoline is the optimal value for tropopause analysis, because it statistically agrees with the thermal tropopause. The selection of the PV threshold is often based on the thermal tropopause. However, a particular PV value may not be appropriate for all isentropes and seasons. Figure 1 shows the zonal and meridional variability of PV at the thermal tropopause, TP_{th}, on 27 April 2003 using European Centre for Medium-Range Weather Forecasts (ECMWF) operational data. Here, PV varies roughly between 0.5 and 7 PVU at the thermal tropo-

[1]Institut für Chemie und Dynamik der Geosphäre: Stratosphäre, Forschungszentrum Jülich, Jülich, Germany.
[2]Also at National Center for Atmospheric Research, Boulder, Colorado, USA.
[3]National Center for Atmospheric Research, Boulder, Colorado, USA.

0148-0227/11/2010JD014343

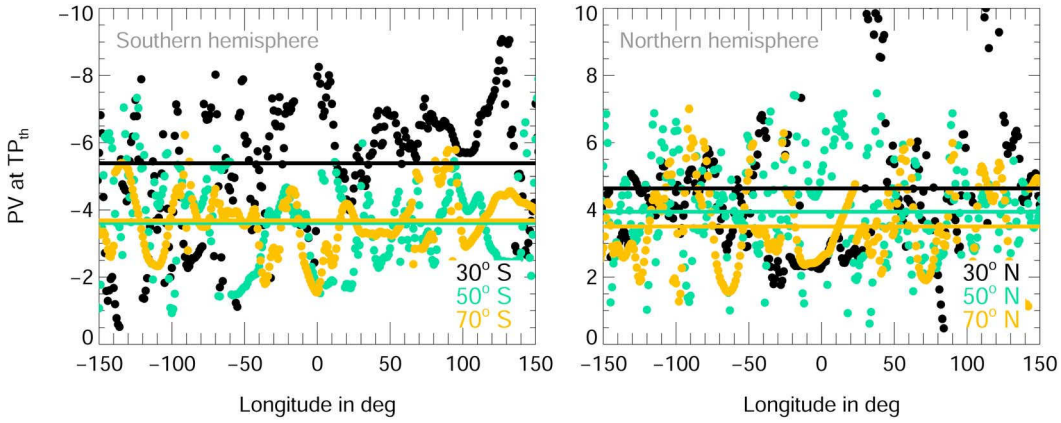

Figure 1. Meridional and zonal variability of PV, calculated from European Centre for Medium-Range Weather Forecasts operational fields, at the thermal tropopause, TP_{th}, depending on different geographical latitudes, i.e., 30° (black), 50° (green), and 70° (orange) on 27 April 2003. The mean $PV_{TP_{th}}$ is marked by solid lines for the different latitudes.

pause between the equator and the pole. The typical values of PV at the thermal tropopause increase toward the equator and are larger than 2 PVU at lower latitudes (e.g., 30°N, black dots). As an alternative, *Randel et al.* [2007] used a series of PV isolines (1–4 PVU) in their studies to indicate the approximate location of the dynamical tropopause. *Kunz et al.* [2009] deduced the mean PV at all thermal tropopause heights at the measurement locations during the SPURT (trace gas transport in the tropopause region) campaigns as $PV_{TP_{th}} \approx 4$ PVU. This mean value is greater than the often used value of $TP_{dyn} = 2$ PVU.

[5] The dynamical tropopause as well as the tropopause region have been analyzed in various ways using properties of the PV field on isentropic surfaces. For example, *Reed* [1955] studied upper level frontogenesis and found a near-discontinuous field of PV which separates high values of PV in the stratosphere from low values in the troposphere. *Shapiro et al.* [1998] introduced the mean potential vorticity (MPV) to describe the PV distribution in the vicinity of the tropopause and to analyze interactions between jet streams at different latitudes. MPV represents a vertical average of PV within a layer bounded by the two isentropic surfaces $\theta = 280$ K and $\theta = 340$ K to capture the tropopause characteristics between the subtropics and the Arctic.

[6] Another method to generalize the dynamical tropopause is the calculation of the isentropic PV gradient [*Hoskins et al.*, 1985]. The distribution of the extratropical PV on each middle world isentropic surface is of interest. The isentropic PV gradient has been used as an indicator for the tropopause in idealized life-cycle experiments when analyzing the transport and mixing of distinct air masses across the tropopause [*Polvani and Esler*, 2007]. Here the quasi-latitudinal PV gradient on isentropic surfaces is sharpest across the jet streams. The pattern of PV takes the form of a narrow band of enhanced PV gradient following the position of the meandering jet stream including perturbations or double jet stream structures [*Schwierz et al.*, 2004; *Martius et al.*, 2010]. These PV gradients are maximized near the jet cores and reflect the existence of barriers to eddy transport across the jet stream [*McIntyre and Palmer*, 1984; *Juckes and McIntyre*, 1987; *Holton et al.*, 1995]. There have been studies concerning the strength of the transport barrier in the tropopause region. *Haynes and Shuckburgh* [2000] used the minimum value of effective diffusivity on each isentropic surface as a measure of the tropopause barrier and as an alternative definition of the tropopause. Also, *Berthet et al.* [2007] defined a "Lagrangian tropopause" based on the number of backward trajectories crossing the tropopause during a fixed time period of 30 days. In their study, only few trajectories cross such a surface, highlighting the transport barrier associated with the tropopause.

[7] Although the importance of PV gradients for the determination of the dynamical tropopause has been discussed, no global determination of the dynamical tropopause based on this concept has been performed. The goal of this work is to present a general method to determine the PV isoline on isentropes that is most appropriate for the dynamical tropopause. On the basis of the isentropic gradient, the method follows a previously developed diagnostic to determine the edge of the polar vortex [*Nash et al.*, 1996; *Steinhorst et al.*, 2005]. *Nash et al.* [1996] calculated the product of isentropic PV gradient and zonal wind speed with equivalent latitude to determine the edge of the polar vortex. A method similar to the Nash criterion is developed in this work to determine the dynamical tropopause. We consider this method to be conceptually more fundamental than using an ad hoc value of PV for the dynamical tropopause. Therefore, the location of the jet streams near the tropopause is of interest, because the isentropic PV gradients maximize in their vicinity [*Martius et al.*, 2010].

[8] The generalized dynamical tropopause on a given isentrope is defined as the PV isoline, where the isentropic PV gradient in equivalent latitude space, constrained by the horizontal wind field, is maximized. The method to define the generalized dynamical tropopause, including a description of equivalent latitude, is presented in section 2. We also introduce an additional parameter to characterize the width of the transition region, indicated by enhanced PV gradients around the dynamical tropopause. This parameter is similar to the boundary parameter of the polar vortex defined by *Nash et al.* [1996]. The spatial and temporal behavior of the PV gradient–based tropopause is examined in section 3

using a daily time series of ECMWF analyses for 2002. A zonal and time mean distribution of the PV at the dynamical tropopause is presented for this time period to provide statistical information for understanding the use of selected PV values as the dynamical tropopause. The implication of the PV distribution at the dynamical tropopause, and the potential application of the boundary parameter, are discussed in section 4.

2. Data and Methodology

2.1. ECMWF Data

[9] Potential vorticity is calculated from the T511L61 operational ECMWF data [*Simmons et al.*, 2005]. The data are interpolated to a 1° × 1° horizontal grid and to 35 vertical pressure levels (19 equidistant levels between 1000 and 100 hPa). The vertical resolution is ~0.8–1.4 km around the extratropical tropopause. These ECMWF data on pressure levels are then interpolated on isentropic θ levels. The focus is on middle world isentropes between 300 and 380K with a discretization of 5 K. The height of the thermal tropopause is identified using the ECMWF vertical temperature profiles on pressure levels and is also interpolated on isentropic levels. The thermal tropopause is defined as the lowest pressure level at which the lapse rate is 2 K km^{-1} or less. The lapse rate should not exceed 2 K km^{-1} between this level and all higher levels within 2 km [*WMO*, 1957].

2.2. Identification of the PV Gradient–Based Dynamical Tropopause

[10] Similar to the polar vortex diagnostic of *Nash et al.* [1996], the PV values on each isentrope are transformed into equivalent latitudes varying between −90°S and 90°N [*Butchart and Remsberg*, 1986]. For each isentrope, the area enclosed by a PV contour in a hemisphere is calculated and transformed to a circle with the same area centered at the pole. Here, the equivalent latitude, φ_e, is the distance in degrees of latitude from the equator to this circle and is given by

$$\varphi_e = \arcsin\left(\frac{1 - A(\mathrm{PV})}{2\pi r^2}\right). \quad (1)$$

The radius of the Earth is r and A(PV) is the area enclosed by the PV contour. The equivalent latitudes φ_e are calculated on the original 1° latitude × 1° longitude grid for a range of isentropes. The method to determine the PV isoline on isentropic surfaces, which represent the dynamical tropopause based on the PV gradients and the horizontal wind speed, is described in the following. As an example, the concept for determining the dynamical tropopause based on isentropic PV gradients is discussed for the case study on 27 April 2003 (Figure 2).

[11] For each isentrope θ, the equivalent latitudes, which depend on the geographical latitude and the geographical longitude, are binned. The bin size of equivalent latitude is 1°, which is the horizontal resolution of the ECMWF data used. The zonal mean in the φ_e space of all desired atmospheric variables (e.g., PV and horizontal wind speed, $u_h = \sqrt{u^2 + v^2}$), is calculated. Note that, according to the definition of the equivalent latitude, there is a one-to-one PV value for each equivalent latitude. Figure 2 shows the PV distribution (Figure 2a) and the horizontal wind speed u_h (Figure 2e) for four different isentropes (300–360 K) against the equivalent latitude, φ_e, in the Northern Hemisphere on 27 April 2003. The PV distribution on each isentrope has an "S" shape and roughly resembles the distribution of the mathematical function $f(x) = \arctan(x)$ (Figure 2i, black line), which increases with x with a point of inflection at $x = 0$.

[12] The gradient of potential vorticity with equivalent latitude as well as the product with the horizontal wind speed are calculated for each isentrope and hemisphere (Figures 2b and 2f). These fields are smoothed with a φ_e = 5° wide running mean to remove noise in their distributions. Figure 2i shows the first derivative $f^1(x)$ (orange line) of the arc tangent function $f(x)$, which shows a maximum where $f(x)$ has its point of inflection. The gradient of potential vorticity with equivalent latitude has a maximum at the point of inflection of the PV distribution.

[13] For each isentrope and hemisphere, the equivalent latitude of the dynamical tropopause, φ_e^{TP}, is defined as the location of the highest potential vorticity gradient, constrained by the wind speed. Mathematically, φ_e^{TP} is given by

$$\varphi_e^{\mathrm{TP}}(\theta) = \varphi_e(\theta)\Big|_{\max\left(\frac{\partial PV(\varphi_e,\theta)}{\partial \varphi_e} \times u_h(\varphi_e,\theta)\right)}. \quad (2)$$

This means that φ_e^{TP} is defined as the equivalent latitude on an isentrope θ at which the product of the PV gradient and the horizontal wind speed (Figure 2f) reaches a maximum. The PV isoline associated with this equivalent latitude, PV^{TP}, is chosen as PV of the dynamical tropopause on a given isentrope.

[14] *Nash et al.* [1996] used the zonal wind speed, u, for the determination of the vortex edge, whereas the horizontal wind speed, u_h, is used here. This horizontal wind speed contains both the meridional and the zonal wind components and thus correctly represents the undulations of the jet streams where the isentropic PV gradients are enhanced. Figure 2 shows φ_e^{TP} as a vertical dashed line for the four isentropes between 300 and 360 K. There may be multiple peaks in the distribution of the PV gradient and the horizontal wind speed; for example, the distribution of both fields on the 320 K isentrope shows two pronounced maxima (Figures 2b and 2e, orange lines). These maxima are most probably due to two separate jet streams. When the product of PV gradients and horizontal wind speed is considered, usually one peak appears in the distribution, which we define as the location of the dynamical tropopause (Figure 2f).

[15] Some restrictions have been applied when determining φ_e^{TP}. The equivalent latitude space for the determination of φ_e^{TP} is restricted to $5° < |\varphi_e| < 85°$. Furthermore, φ_e^{TP} is searched within the PV range $0.5 < |\mathrm{PV}(\varphi_e, \theta)| < 7$ PVU (see shaded area in Figure 2a). This PV range covers the variability of PV at the thermal tropopause (Figure 1).

2.3. Determination of the Transition Region Around the Dynamical Tropopause

[16] The original Nash criterion [*Nash et al.*, 1996] includes the definition of a boundary region between the local maximum convex and concave curvature of the PV distribution surrounding the polar vortex edge. Similarly, we

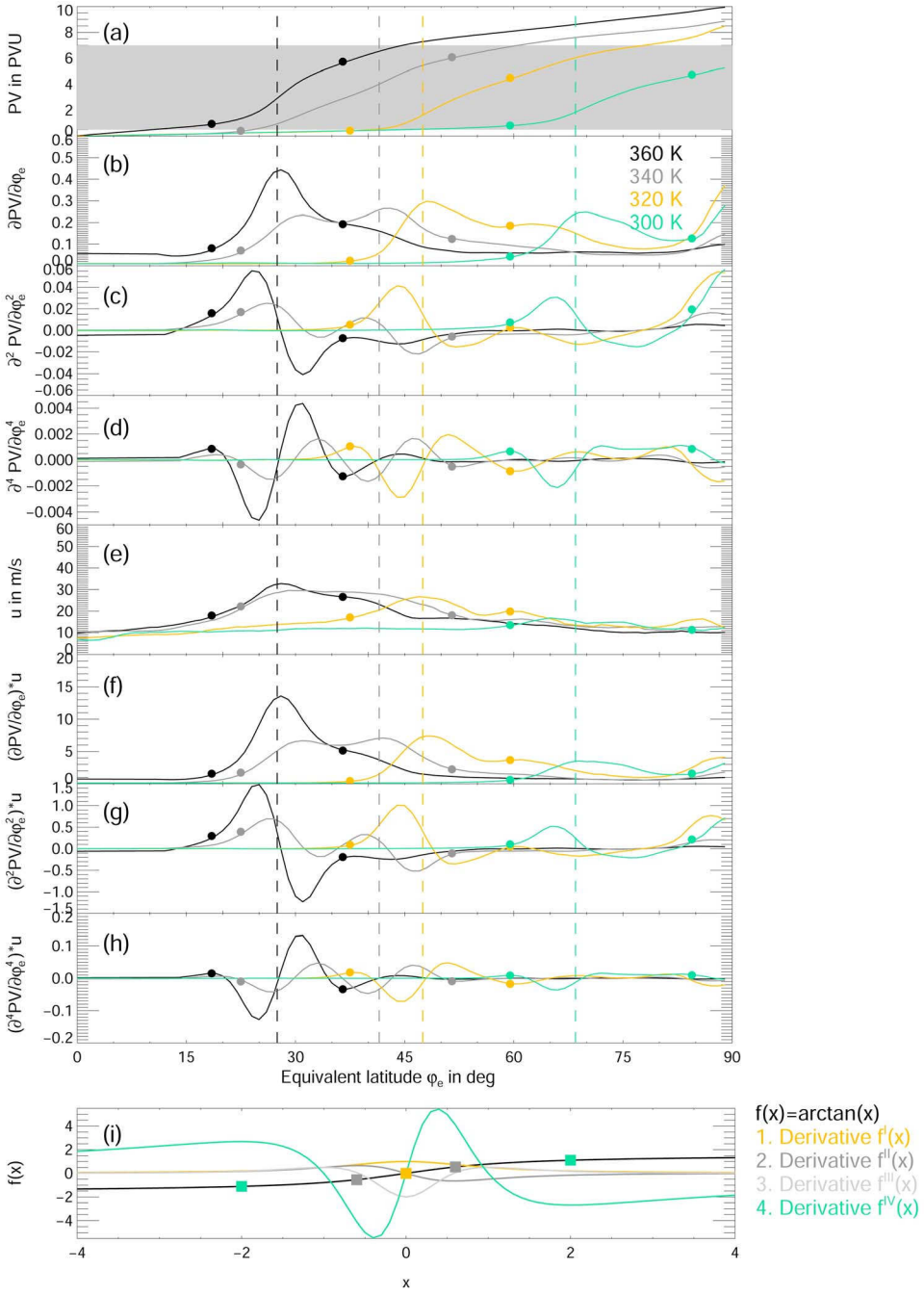

Figure 2. (a) Distribution of PV on the isentropes 300 K (green), 320 K (gold), 340 K (gray), and 360 K (black) against equivalent latitude in the Northern Hemisphere for 27 April 2003. The PV gradient, i.e., (b) the first derivative of PV, on these isentropes, (c) the second derivative of PV, (d) the fourth derivative of PV, and (e) the horizontal wind speed are shown. The product of the horizontal wind speed (f) with the PV gradient, (g) with the second derivative, and (h) with the fourth derivative are also shown. The equivalent latitudes of the dynamical tropopause, φ_e^{TP} (vertical dashed lines), and of the transition region, φ_e^{B} (two dots), are shown for each isentrope. (i) An idealized example of the isentropic PV distribution with PV approximated by $f(x) = \arctan(x)$ (black line) is shown; the first four derivatives of $f(x)$ are shown as colored lines. The slope of $f(x)$ is largest where $f^{\mathrm{I}}(x)$ has a maximum. The equivalent latitude at this maximum is defined as dynamical tropopause φ_e^{TP} (orange square at $f(x)$). The slope of $f(x)$ monotonically decreases in both directions of the jet core toward zero. The slope is sufficiently steep where $f^{\mathrm{IV}}(x)$ has local extrema which are defined as the equivalent latitudes of the boundaries φ_e^{B} (green squares at $f(x)$).

introduce a transition region that characterizes the width of enhanced PV gradient separating the troposphere from the stratosphere. Thus, the equivalent latitudes, φ_e^B, as well as the associated PV isolines, PV^B, which limit this transition region around the dynamical tropopause on isentropes θ are defined. This transition region captures different parts of the jet streams, including undulations and jet streaks, which are characterized by a larger spatial extent of high PV gradient.

[17] *Nash et al.* [1996] defined their boundary region by the second derivative of the PV distribution; see also $f^{\mathrm{II}}(x)$ (Figure 2i). For this purpose, the second derivative of PV can be calculated (Figure 2c) and the maximum convex or concave curvature is determined by its product with the horizontal wind speed (Figure 2g). However, our investigations show that a better measure of enhanced PV gradients in the vicinity of jet streams is given by the distance between the local maximum convex and concave curvature of the fourth derivative of the PV distribution. The fourth derivative of the PV distribution is calculated (Figure 2d) and is multiplied by the horizontal wind speed (Figure 2h). The local maximum convex and concave curvature of this fourth derivative of PV multiplied by the horizontal wind speed,

$$\frac{\partial^4 PV(\varphi_e,\theta)}{\partial \varphi_e^4} \times u_h(\varphi_e,\theta), \tag{3}$$

defines the locations of the two equivalent latitudes, φ_e^B, or the associated PV isolines, PV^B, which surround the transition region around the dynamical tropopause. This transition region includes enhanced PV gradients compared to the troposphere and stratosphere on the isentropes. The fourth derivative, $f^{\mathrm{IV}}(x)$, of the function $f(x)$ shows these extrema at the locations where the slope of $f(x)$ approaches zero (see Figure 2i, green squares). The two equivalent latitudes of the transition region boundaries, φ_e^B, are highlighted in Figure 2.

[18] The PV isolines, determined by the fourth derivative of PV, enclose an area, which is much more consistent with the spatial extent of the jet streams and the region of enhanced PV gradient than those based on the second derivative of PV. Generally, the use of the fourth derivative enlarges the transition region compared to the criterion based on the second derivative of PV. The extrema in the fourth derivative mark where PV starts or stops increasing with equivalent latitude. This feature is also demonstrated by the arc tangent example in Figure 2i. The extrema of the fourth derivative of $f(x)$ (Figure 2i, green squares) border the regions with a sufficiently steep first derivative $f^{\mathrm{I}}(x)$.

[19] Figure 3 shows an instantaneous distribution of the horizontal wind speed and PV on the 340 K isentrope in the Northern Hemisphere. The PV isolines representing the dynamical tropopause, PV^{TP}, and those surrounding the transition region, PV^B, are shown. The instantaneous wind speed at 340 K shows a jet stream with a strongly meandering shape. There are two distinct jet streams (subtropical and polar) on this isentrope. In that case, PV^{TP} sometimes coincides with the high wind speed pattern and sometimes it is in between two split parts of a jet stream, and coincides with a high PV gradient in this area. PV^B limits the area of enhanced PV gradients very well. Areas with strongly meandering jet streams as well as jet streaks are characterized by a broader transition on an isentrope. The transition region on the 360 K isentrope surrounding the subtropical jet stream in a rather zonal direction is narrower than on the 340 K isentrope. In this case, the dynamical tropopause coincides very well with the maximum in the wind speed. On the basis of the narrower transition region with a smaller spatial extent of enhanced PV gradient, we suggest that the tropopause is sharper on the 360 K isentrope than on the 340 K isentrope.

3. Results

[20] As indicated by the example in Figure 3, different PV values represent the gradient-based dynamical tropopause on different isentropic surfaces. In this example, PV^{TP} is around 4.15 PVU on the 340 K isentrope, and it is around 3.15 PVU on the 360 K isentrope. To examine the temporal and spatial variability of PV^{TP} statistically, we present an analysis using 1 year of ECMWF data. Specifically, we examine the spatial variation of PV^{TP} in both latitude and equivalent latitude space. We also present the averages and the distributions of PV values at the dynamical tropopause.

3.1. Seasonality of the Dynamical Tropopause

[21] Figure 4 shows the seasonal mean distribution of the horizontal wind speed u_h in m s^{-1} and PV in PVU in the Northern Hemisphere in 2002 on the 340 K isentrope. Figure 4 also shows the seasonal mean of PV^{TP} and PV^B. The seasons are organized according to the Northern Hemisphere: spring (MAM), summer (JJA), autumn (SON), and winter (DJF). There is a seasonal variation of PV^{TP}. It is highest during summer and autumn, around 3.2 PVU, and lowest during spring (2.0 PVU) and winter (2.6 PVU). In the seasonal mean, the dynamical tropopause coincides very well with the jet stream on the 340 K isentrope. Nevertheless, in a few situations when the mean jet stream splits into two or more parts, the dynamical tropopause connects regions of high wind speeds, e.g., around 60°W longitude during spring.

[22] The strength and location of the jet stream also have a seasonal cycle, with higher wind speeds and a more equatorward position in winter than in summer. The behavior of the 2002 jet stream in each season is consistent with the jet stream climatology for the period 1979–1993 given by *Koch et al.* [2006]. The zonal behavior of the jet stream during winter 2002 between the longitudes 0°E and 180°E, as well as its two breaks at the longitudes 30°W and 120°W and the three split parts of the jet stream in spring 2002 agree very well with the climatology. This shows that the selected year, 2002, fits the climatological behavior of the jet stream and it may be used for demonstrating the proposed method for the dynamical tropopause determination.

[23] It is well known that the jet stream is weaker in summer than in winter. Consequently, the transition region of enhanced PV gradients spans a larger region, which has a similar extent around the globe, indicating a less sharp tropopause in the summer months. It reflects the larger permeability between the troposphere and the stratosphere in summer, which leads to a frequent quasi-isentropic cross-tropopause transport of trace gases in that season [e.g.,

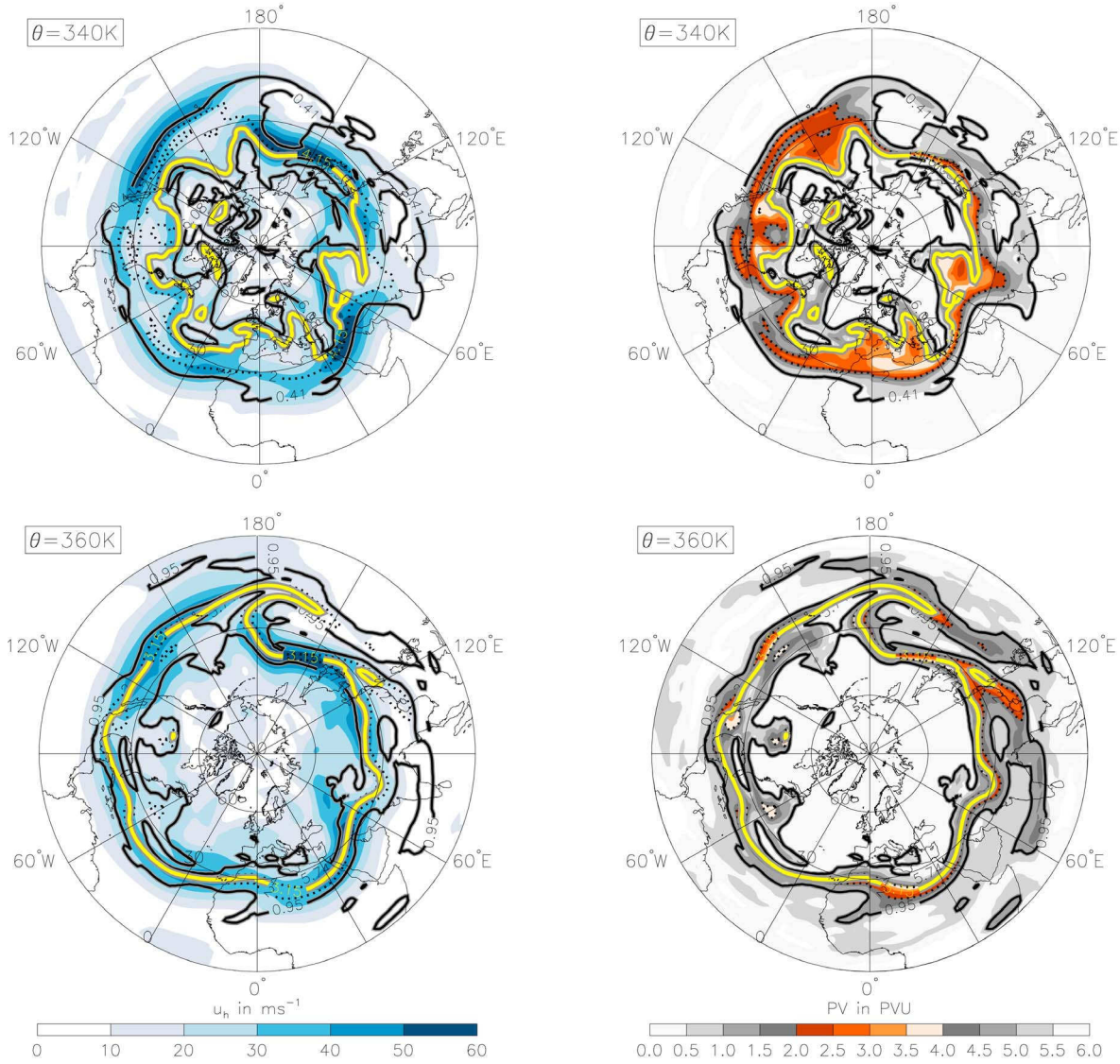

Figure 3. Instantaneous features in the Northern Hemisphere on the (top) 340 K isentrope and (bottom) 360 K isentrope at 1200 UTC, 27 April 2003; (left) horizontal wind speed u_h in m s^{-1} and (right) PV in PVU. PV at the dynamical tropopause is shown in yellow, with PV^{TP} = 4.15 PVU on the 340 K isentrope and PV^{TP} = 3.15 PVU on the 360 K isentrope. PV isolines surrounding the transition region, φ_e^B, are in black. The 2 PVU and 4 PVU isolines are highlighted as thin black dotted lines.

Chen, 1995]. During winter, the transition region has a similar equivalent latitude space between the longitudes 0°W and 180°W. Between the longitudes 180°E and 360°E, where the jet stream is very zonal and strong, the transition region is very narrow. In that region the tropopause is very sharp and acts as a strong barrier to cross-tropopause transport.

[24] Figure 5 shows the mean analysis of the horizontal wind speed and PV fields on 340 K for the Southern Hemisphere. Consistent with the work of *Koch et al.* [2006], the jet stream has a more zonal symmetric form persisting during all seasons. There is also a seasonal cycle of maximum wind speed, but it is not as large as in the Northern Hemisphere. PV^{TP} also shows a seasonal cycle. The value of PV^{TP} for each season is similar to the Northern Hemisphere value, but the isoline has a more zonal shape similar to the jet structure in the Southern Hemisphere. The latitudinal extent of the transition region is almost the same throughout the year. There is no large meridional elongation of the jet stream in the Southern Hemisphere. This behavior is consistent with a weaker seasonal cycle of the tropopause sharpness and the barrier effect compared to the Northern Hemisphere. This result may be compared to the study of *Haynes and Shuckburgh* [2000], who characterized the tropopause barrier close to the jet streams using the effective diffusivity concept. In their study, the spatial extent of low effective diffusivity on the 330 K isentrope has a larger variability in the Northern Hemisphere compared to the Southern Hemisphere.

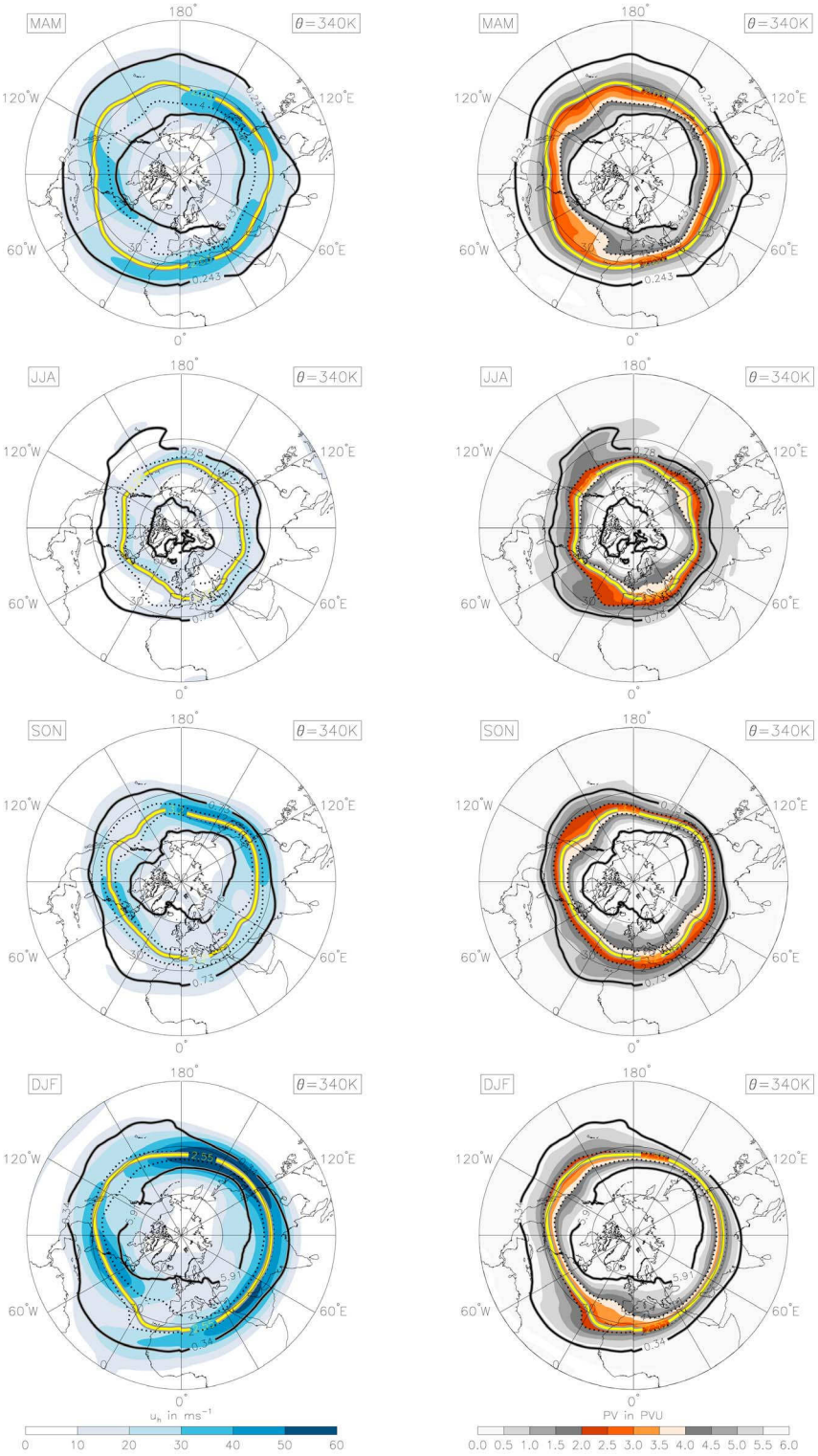

Figure 4. (left) Seasonal mean horizontal wind speed, u_h, in ms $^{-1}$ and (right) PV in PVU in the Northern Hemisphere for 2002 on the 340 K isentrope. Seasons are defined as spring (MAM), summer (JJA), autumn (SON), and winter (DJF). Mean PV at the dynamical tropopause, PV^{TP} (yellow), and around the transition region, PV^{B} (black lines), are shown together with the average 2 PVU and 4 PVU isolines (black dotted lines).

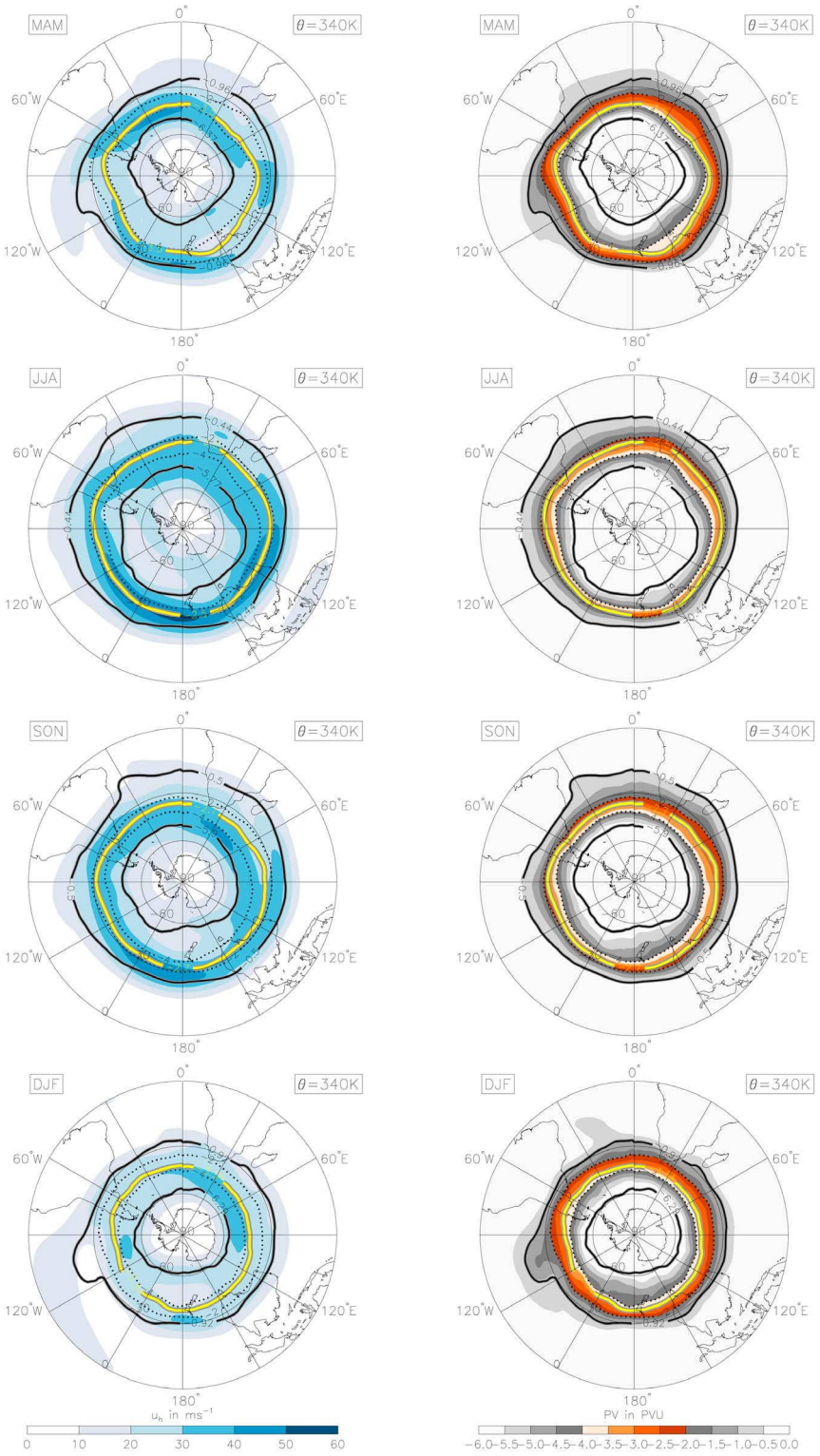

Figure 5. Seasonal mean horizontal wind speed and PV as in Figure 4 but for the Southern Hemisphere.

3.2. Zonal Mean Distribution of the Dynamical Tropopause

[25] Figure 6 shows the zonal and seasonal mean of PV in equivalent latitude for the potential temperature range between 300 and 380 K in 2002. For each isentrope, the seasonal mean equivalent latitude of the dynamical tropopause, φ_e^{TP}, is shown together with the transition region of enhanced PV gradient, φ_e^{B}.

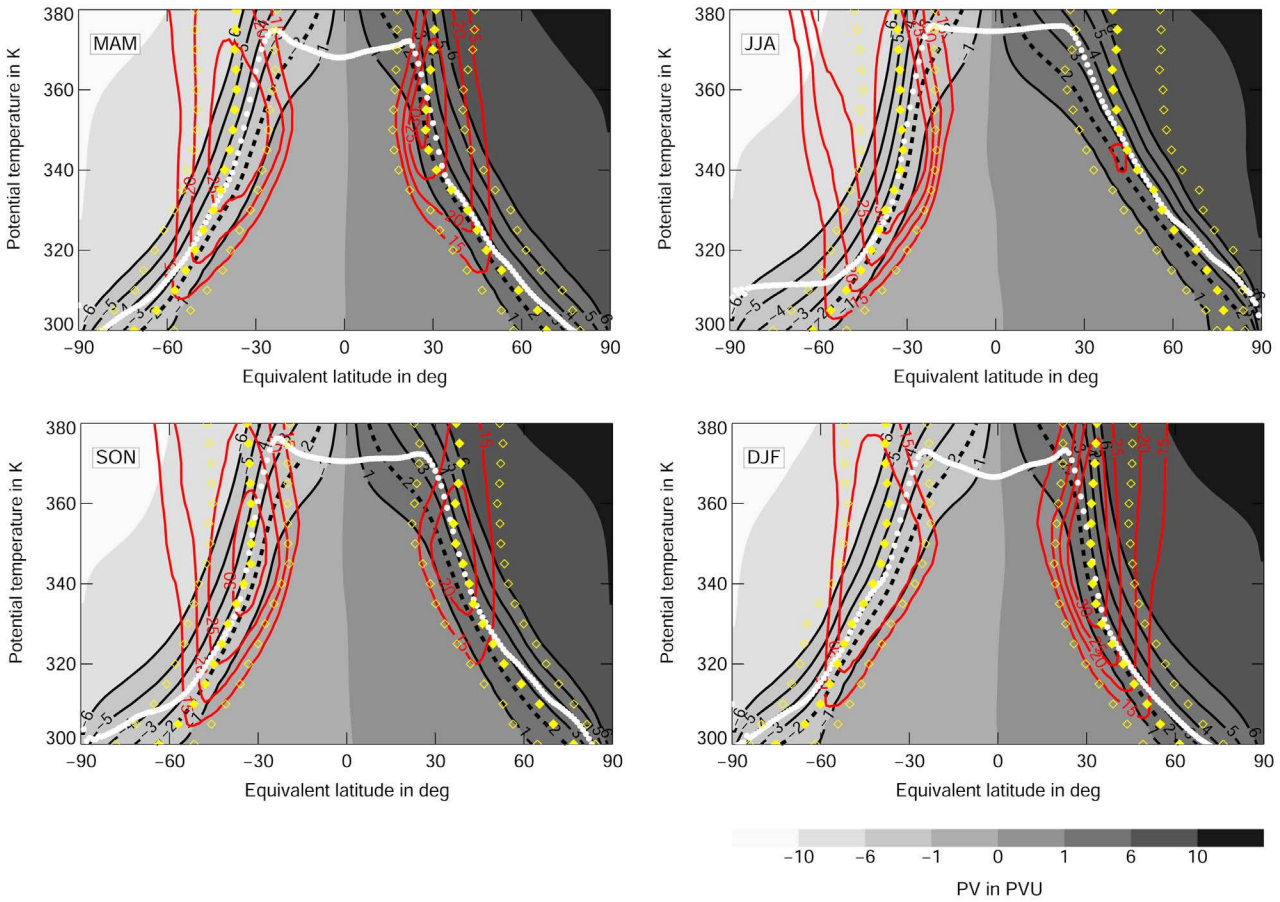

Figure 6. Zonal mean PV in PVU with equivalent latitude for different seasons in 2002. The dynamical tropopause, φ_e^{TP} (yellow diamonds), and the transition region, φ_e^{B} (open yellow diamonds), are shown on each isentrope. The height of the thermal tropopause, $\theta_{TP_{th}}$, is shown by white dots. Specific PV isolines between ±1 and ±6 PVU are highlighted by black solid lines. The 2 PVU isoline is a black dashed line and the zonal wind is shown in red.

[26] In the vicinity of the subtropical jet stream, the dynamical tropopause on all isentropes coincides on average very well with the maximum wind speed in the center of the jet stream. The dynamical tropopause is also very close to the thermal tropopause in this area. Toward the poles on lower isentropes, the two tropopauses deviate, with the thermal tropopause at a higher equivalent latitude than the dynamical tropopause. On the contrary, toward the equator on higher isentropes, the thermal tropopause is at a lower equivalent latitude than the dynamical tropopause. This is most obvious on isentropes higher than 350 K above the jet core. Here, φ_e^{TP} rather represents the wind maximum connected with the subtropical jet stream. On these isentropes, there is usually one pronounced maximum in the wind speed distribution combined with one pronounced maximum in the PV gradient distribution with equivalent latitude. This has an effect on the calculation of φ_e^{TP}.

[27] The difference between the two tropopauses in the extratropics is largest on isentropes lower than 310 K. Lower isentropes may be affected by cyclonic and anticyclonic systems in the upper troposphere, with the cyclonic systems most frequently connected with a thermal tropopause above the dynamical tropopause defined by the 2 PVU isosurface [*Wirth*, 2000, 2001]. A prevalence of cyclonic systems in the midlatitudes can influence the behavior of the higher thermal tropopause compared to the dynamical tropopause in the zonal mean picture (Figure 6). During Southern Hemisphere winter (JJA), both tropopauses deviate, especially near the South Pole. In that region, the thermal tropopause remains approximately constant on the 310 K isentrope for equivalent latitudes lower than −60°S. This behavior of the thermal tropopause, which is also observed in other zonal mean studies [e.g., *Birner*, 2006], may well be due to the onset and buildup of the polar vortex. At that time, the South Pole region cools and the isentropes ascend toward the pole relative to the pressure levels, and the isentropic level of the thermal tropopause stops decreasing toward the pole.

[28] On a seasonal average basis, the PV gradient-based dynamical tropopause does not coincide with the 2 PVU isoline (Figure 6). This difference is greater in summer (JJA in the Northern Hemisphere, DJF in the Southern Hemisphere) than in winter and it is most pronounced on isentropes between 310 and 350 K. This finding is similar to the finding by *Berthet et al.* [2007], who also showed a

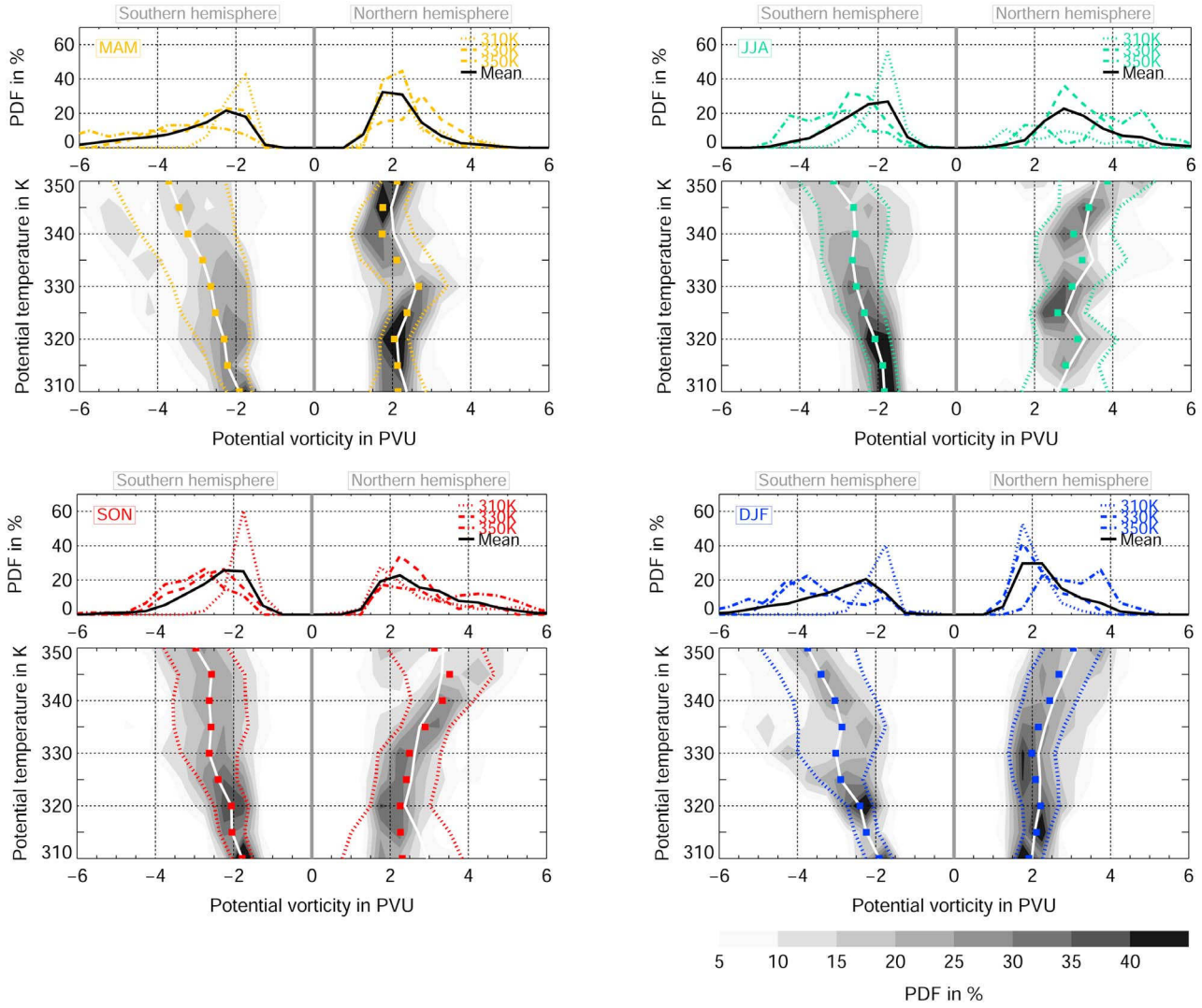

Figure 7. Seasonal probability distribution functions (PDFs) of PV^{TP} on middle world isentropes (gray shading) for 2002. The mean (solid white line), the median (solid squares), and the standard deviation (dotted lines) of PV^{TP} per 5 K bins are shown. The PDF of PV^{TP} on single isentropes 310, 330, and 350 K as well as the mean PDF of PV^{TP} for all isentropes between 310 and 350 K (black lines) are shown in the small panels, respectively.

remarkable difference between the position of their Lagrangian tropopause and the 2 PVU isosurface.

[29] The meridional extent of the transition region is similar for all isentropes in the Southern Hemisphere. In the Northern Hemisphere, the meridional extent is larger during summer than during winter on higher isentropes characteristic of the subtropical jet stream. This again may reflect the permeability of the jet stream connected with a larger width of enhanced PV gradient during summer compared to winter.

[30] In the following, some further statistical analyses regarding the variability of PV at the dynamical tropopause on isentropes between 310 and 350 K are presented.

3.3. PDF of the Dynamical Tropopause PV

[31] Figure 7 shows the seasonal probability distribution functions (PDFs) of PV^{TP} on each isentrope for the 310–350 K range. The mean, the median, and the standard deviation of the PDF of PV^{TP} are shown. PV at the dynamical tropopause increases from lower isentropes to higher isentropes in all seasons and in both hemispheres, which is clearly shown by the means and the medians of the distribution. This increase is observed for all seasons with the exception of Northern Hemisphere spring (MAM). In the Southern Hemisphere, the PV at the dynamical tropopause increases above the entire range of isentropes (310–350 K), but in the Northern Hemisphere this increase is more obvious above the 330 K isentrope for all seasons. It should be noted that, on isentropes higher than 330 K, PV^{TP} represents the tropopause in the subtropics rather than in the midlatitudes and polar regions. For these regions in higher geographical latitudes PV^{TP} is usually found on isentropes lower than 330 K.

[32] In both hemispheres, there is a larger dispersion of PV^{TP} around its mean and median during summer (JJA for Northern Hemisphere, DJF for Southern Hemisphere) and

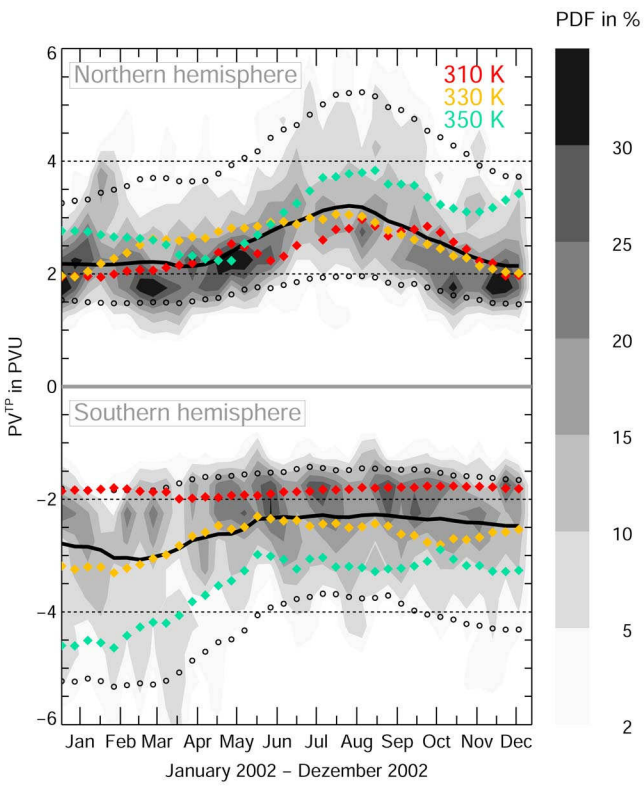

Figure 8. PDF of the 2002 time series of PV^{TP} on middle world isentropes between 310 and 350 K (gray shading) for the two hemispheres. The bin size for the time is 10 days and for PV it is 0.5 PVU. The median of the total PDF (black solid line), the median of the PDF on the three isentropes (colored symbols), and the 5th and 95th percentiles of the PDF (black open circles) are shown.

autumn (SON for Northern Hemisphere, MAM for Southern Hemisphere) than during winter (DJF for Northern Hemisphere, JJA for Southern Hemisphere) and spring (MAM for Northern Hemisphere, SON for Southern Hemisphere). This is clearly shown by the standard deviation, which indicates that the dispersion of PV^{TP} may be twice as large in summer than in winter. The dispersion of PV^{TP} increases with the height of the isentrope. This increase is again more pronounced in the Southern Hemisphere. The shape of the PDF does not vary with season in the Southern Hemisphere as much as in the Northern Hemisphere. This is also evident by the median and the mean PDF of PV^{TP}, which are the same for each isentrope in the Southern Hemisphere. This is not observed in the Northern Hemisphere. Especially during boreal summer there is a large dispersion of PV^{TP} on each isentrope and the value of the mean and the median of PV^{TP} may be slightly different on some isentropes. This may be due to stronger undulations of the jet streams in the Northern Hemisphere, which span a larger meridional range. In the Southern Hemisphere, the subtropical jet stream has a more stable and continuous position, which is due to the lack of land masses in this hemisphere.

[33] Figure 7 also shows the PDF of PV^{TP} on three different isentropes, 310, 330, and 350 K, as well as the total mean PDF of PV^{TP} for the entire isentropic range from 310 to 350 K. Here, the total mean PDF of PV^{TP} represents a 3-D PV isosurface in the atmosphere between 310 and 350 K, which defines the dynamical tropopause for the entire isentropic range. However, the mean PDF of PV^{TP} on the single isentropes represents a PV isoline most appropriate for the respective isentrope. There is no large seasonal variation of the total mean PDF of PV^{TP}. The total mean PDF roughly maximizes in the vicinity of the 2 PVU isoline. This maximum is slightly away from the 2 PVU isoline in winter and in summer in the Northern Hemisphere. The seasonal PDF on the single isentropes shows a significant difference from the total mean PDF for each season. There is a larger seasonal variability of the maximum of the PDF of PV^{TP} on each isentrope in the Northern Hemisphere than in the Southern Hemisphere.

[34] To further characterize the seasonal variation of PV^{TP}, Figure 8 provides the PDF of PV^{TP} for all isentropes between 310 and 350 K as a time series for the year 2002 for both hemispheres. Here the PDF is calculated using 10 day time bins. On both hemispheres, the seasonal cycle of PV^{TP} shows higher values during summer and lower values during winter. The 5th and 95th percentiles of PV^{TP} on all isentropes indicate a variation between 1.5 and 5 PVU in both hemispheres throughout the year. The seasonal cycle including all isentropes between 310 and 350 K is more pronounced in the Northern Hemisphere, when the difference between the median PDF of PV^{TP} from summer to winter is larger than in the Southern Hemisphere. The seasonal cycle of the median PDF of PV^{TP} is larger on higher isentropes than on lower isentropes in both hemispheres. Almost no seasonal cycle is present on the 310 K isentrope in the Southern Hemisphere. This is also seen in other years, including 2003 and 2004 (not shown).

[35] There is a small day-to-day variability in PV^{TP}. We have performed a temporal variance analysis using a method discussed by *Kunz et al.* [2008]. The result shows that the variance of PV^{TP} enhances at time scales between 10 and 360 days and the variability is larger at the interseasonal and seasonal time scales than at the daily time scale. This implies that the value of PV^{TP} is relatively stable at lower time scales and the atmospheric processes influencing the position of the dynamical tropopause on an isentrope are on a seasonal time scale. These can be quasi-isentropic troposphere to stratosphere exchange processes or convective processes, which have a significant seasonal cycle.

[36] Figures 7 and 8 clearly show that the PV gradient-based dynamical tropopause can be different from the one inferred from an ad hoc value of PV. There is a seasonal and a spatial variation of PV representative of the dynamical tropopause. Figures 7 and 8 may be used to decide whether the PV isoline, which is used to define the dynamical tropopause, is appropriate for a given question of scientific interest.

4. Summary

[37] We have presented a method to determine a PV isoline on isentropes most appropriate for defining the extratropical dynamical tropopause based on isentropic PV gradients. This is an alternative approach to using an ad hoc

PV value for the dynamical tropopause in the entire extratropics, without any distinction regarding isentropes and seasons. Our analysis considers the seasonal and spatial variability of the dynamical tropopause and its impact on the tropopause representative PV isoline on isentropes. The equivalent latitude of the maximized product of PV gradient with horizontal wind speed, φ_e^{TP}, on different middle world isentropes is calculated. This equivalent latitude, or the corresponding PV isoline, PV^{TP}, defines the location of the PV gradient-based dynamical tropopause. The transition region on isentropes around the dynamical tropopause, which is characterized by enhanced PV gradients compared to the rest of the troposphere or stratosphere, is also introduced. The PV isolines which limit this transition region, $PV^{\mathcal{B}}$, include the region characterized by jet stream undulations and jet streaks. Conceptually, the width of the transition region represents the sharpness of the tropopause defined on isentropes. The validity of this boundary parameter will be examined by analyzing chemical tracers in future studies.

[38] A statistical analysis of PV^{TP} is performed for extratropical isentropes between 310 and 350 K. Here the PV representing the dynamical tropopause has a large seasonal cycle, with higher values during summer and lower values during winter in both hemispheres. The results show that PV^{TP} varies between 1.5 and 5 PVU in both hemispheres throughout the year on the isentropes between 310 and 350 K. The seasonal cycle increases with the height of the isentropes. In 2002, a clear seasonal cycle is observed for each isentropic level between 310 and 350 K, except for 310 K in the Southern Hemisphere. On this isentrope, the particular PV value of 2 PVU represents the dynamical tropopause throughout the year.

[39] The Southern Hemisphere shows a sharper increase of PV representative for the dynamical tropopause from lower isentropes to higher isentropes than the Northern Hemisphere. Higher isentropes represent the tropopause in the subtropics and midlatitudes, and lower isentropes represent the tropopause in higher latitudes. The sharper increase of PV at the dynamical tropopause in the Southern Hemisphere may be due to the more stable position of the subtropical jet stream compared to the Northern Hemisphere, where the jet stream spans a larger meridional region due to its meandering shape. This is consistent with the result of the effective diffusivity analysis [*Haynes and Shuckburgh*, 2000], where the subtropical jet stream in the Southern Hemisphere is seen as a strong barrier to cross-tropopause transport throughout the year. However, in the summer the Northern Hemispheric jet stream has a weaker barrier effect. This has an influence on the property of the dynamical tropopause. Thus, there is a large dispersion of PV^{TP} on a range of isentropes in Northern Hemisphere summer. The dispersion in summer is twice that in winter.

[40] This analysis suggests that the PV value representing the dynamical tropopause is a variable dependent on isentropes and seasons in the respective hemisphere. The temporal and spatial variation of PV^{TP} on isentropes should be taken into account when doing atmospheric analyses using the dynamical tropopause. Nevertheless, an analysis of observed tracer distributions around this PV gradient-based dynamical tropopause is still necessary to demonstrate the application of this new concept for diagnosing transport and mixing across a transport barrier.

[41] **Acknowledgments.** This work is supported in part by EOS, a program of the Helmholtz Association of German Research Centres, and by the German Academy of Sciences Leopoldina (support code LPDS 2009–25). Thanks go to Heini Wernli and two anonymous reviewers for their constructive criticisms. We further thank Thomas Birner, Leigh Munchak, Jeffrey Taylor, and Juan Antonio Añel for their helpful comments on an earlier version of the manuscript.

References

Berthet, G., J. G. Esler, and P. H. Haynes (2007), A Lagrangian perspective of the tropopause and the ventilation of the lowermost stratosphere, *J. Geophys. Res.*, *112*, D18102, doi:10.1029/2006JD008295.

Birner, T. (2006), Fine-scale structure of the extratropical tropopause region, *J. Geophys. Res.*, *111*, D04104, doi:10.1029/2005JD006301.

Butchart, N., and E. E. Remsberg (1986), The area of the stratospheric polar vortex from analyzed winds, *J. Atmos. Sci.*, *43*, 1319–1339.

Chen, P. (1995), Isentropic cross-tropopause mass exchange in the extratropics, *J. Geophys. Res.*, *100*(D8), 16,661–16,673.

Ertel, H. (1942), Ein neuer hydrodynamischer Wirbelsatz, *Meteorol. Z.*, *59*(9), 277–281.

Haynes, P., and E. Shuckburgh (2000), Effective diffusivity as a diagnostic of atmospheric transport: 2. Troposphere and lower stratosphere, *J. Geophys. Res.*, *105*(D18), 22,795–22,810.

Hoerling, M. P., T. K. Schaack, and A. J. Lenzen (1991), Global objective tropopause analysis, *Mon. Weather Rev.*, *119*, 1816–1831.

Hoinka, K. P. (1997), The tropopause: Discovery, definition and demarcation, *Meteorol. Z.*, *6*, 281–303.

Holton, J. R., P. H. Haynes, M. E. McIntyre, A. R. Douglass, R. B. Rood, and L. Pfister (1995), Stratosphere-troposphere exchange, *Rev. Geophys.*, *33*, 403–440.

Hoskins, B. J., M. E. McIntyre, and A. W. Robertson (1985), On the use and significance of isentropic potential-vorticity maps, *Q. J. R. Meteorol. Soc.*, *111*, 877–946.

Juckes, M. N., and M. E. McIntyre (1987), A high resolution one-layer model of breaking planetary waves in the stratosphere, *Nature*, *328*, 590–596.

Koch, P., H. Wernli, and H. Davies (2006), An event-based jet-stream climatology and typology, *Int. J. Climatol.*, *26*, 283–301.

Kunz, A., C. Schiller, F. Rohrer, H. G. J. Smit, P. Nedelec, and N. Spelten (2008), Statistical analysis of water vapour and ozone in the UT/LS observed during SPURT and MOZAIC, *Atmos. Chem. Phys.*, *8*, 6603–6615.

Kunz, A., P. Konopka, R. Müller, L. L. Pan, C. Schiller, and F. Rohrer (2009), High static stability in the mixing layer above the extratropical tropopause, *J. Geophys. Res.*, *114*, D16305, doi:10.1029/2009JD011840.

Martius, O., C. Schwierz, and H. C. Davies (2010), Tropopause-level waveguides, *J. Atmos. Sci.*, *67*, 866–879, doi:10.1175/2009JAS2995.1.

McIntyre, M. E., and T. N. Palmer (1984), The "surf zone" in the stratosphere, *J. Atmos. Terr. Phys.*, *46*, 825–849.

Nash, E. R., P. A. Newman, J. E. Rosenfield, and M. R. Schoeberl (1996), An objective determination of the polar vortex using Ertel's potential vorticity, *J. Geophys. Res.*, *101*(D5), 9471–9478.

Polvani, L. M., and J. G. Esler (2007), Transport and mixing of chemical air masses in idealized baroclinic life cycles, *J. Geophys. Res.*, *112*, D23102, doi:10.1029/2007JD008555.

Randel, W. J., D. J. Seidel, and L. L. Pan (2007), Observational characteristics of double tropopauses, *J. Geophys. Res.*, *112*, D07309, doi:10.1029/2006JD007904.

Reed, R. J. (1955), A study of a characteristic type of upper-level frontogenesis, *J. Meteorol.*, *12*, 226–237.

Schwierz, C., S. Dirren, and H. C. Davies (2004), Forced waves on a zonally aligned jet stream, *J. Atmos. Sci.*, *61*, 73–87.

Shapiro, M. A., H. Wernli, J.-W. Bao, J. Methven, X. Zou, J. D. Doyle, T. Holt, E. Donall-Grell, and P. J. Neiman (1998), A planetary-scale to mesoscale perspective of the life cycles of extratropical cyclones: The bridge between theory and observations, in *The Life Cycles of Extratropical Cyclones*, edited by S. Grønås and M. A. Shapiro, pp. 139–185, Am. Meteorol. Soc., Boston, Mass.

Simmons, A., M. Hortal, G. Kelly, A. McNally, A. Untch, and S. Uppala (2005), ECMWF analyses and forecasts of stratospheric winter polar vortex breakup: September 2002 in the Southern Hemisphere and related events, *J. Atmos. Sci.*, *62*, 668–689.

Steinhorst, H.-M., P. Konopka, G. Günther, and R. Müller (2005), How permeable is the edge of the Arctic vortex: Model studies of winter 1999–2000, *J. Geophys. Res.*, *110*, D06105, doi:10.1029/2004JD005268.

Wirth, V. (2000), Thermal versus dynamical tropopause in upper-tropospheric balanced flow anomalies, *Q. J. R. Meteorol. Soc.*, *126*, 299–317.

Wirth, V. (2001), Cyclone-anticyclone asymmetry concerning the height of the thermal and dynamical tropopause, *J. Atmos. Sci.*, *58*, 26–37.

World Meteorological Organization (WMO) (1957), Meteorology—A three-dimensional science, *WMO Bull.*, *6*, 134–138.

World Meteorological Organization (WMO) (1986), Atmospheric ozone, *Rep. 16*, Geneva, Switzerland.

P. Konopka, A. Kunz, and R. Müller, Institut für Chemie und Dynamik der Geosphäre: Stratosphäre, Forschungszentrum Jülich, D-52425 Jülich, Germany. (a.kunz@fz-juelich.de)

L. L. Pan, National Center for Atmospheric Research, Boulder, CO 80305, USA.